# Performance Analysis and Comparison for Two Topologies of Flux-Switching Permanent Magnet Machine

Xu Zhang, Wei Zhang, *Member, IEEE*, Xingyan Liang and Ping Lu

***Abstract*—Flux-switching permanent magnet (FSPM) machine is a kind of stator-typed permanent magnet machine, which is suitable for driving electric vehicles and hybrid electric vehicles because of their large power/torque density and high efficiency. The axial field flux-switching permanent magnet machine (AFFSPMM) and radial field flux-switching permanent magnet machine (RFFSPMM) with H-typed iron cores are reached and compared in this paper. On the condition of the same outer diameters and total volumes, the electromagnetic performances of the two machines are analyzed and compared by the three-dimensional finite element method，including the air gap flux density, inductance, back electromotive force (EMF), electromagnetic torque and loss. The finite element results show that the copper loss of AFFSPMM is higher than that of RFFSPMM at the rated load, however, the total loss of AFFSPMM is lower than that of the RFFSPMM. Meanwhile, AFFSPMM has greater torque than RFFSPMM in the constant power range. The related experiments are done to validate the finite element results, which are basically consistent with experiment results.**

***Index Terms*—Flux-switching permanent magnet machine, finite element method, electromagnetic characteristics, torque, loss.**

## I. INTRODUCTION

ENERGY and environmental issues have become two major factors that constraint the development of automobiles. The development of new energy vehicles can solve the problem [1]. As we all known, driving motors is one of the crucial components in vehicles. At present, the main driving motors include induction motors, permanent magnet motors and switched reluctance motors [2]. In order to meet the requirements of large torque density, wide speed range, and good fault tolerance of driving motors in the application of new energy vehicles [3]-[4], different topologies of driving machines are researched and developed. Among them, flux-switching permanent magnet (FSPM) machine is a double salient machine which exhibits the advantages of large output torque, high efficiency and good fault tolerant capability [5], so it has become a hot research direction in recent years. The FSPM machine is mainly divided into radial field flux-switching permanent magnet machine (RFFSPMM) and axial field flux-switching permanent magnet machine (AFFSPMM).

E. Hoang firstly proposed the concept of flux-switching in 1997. In view of the problem of the large amount of permanent magnets used in the traditional stator-typed RFFSPMM shown in Fig. 1(a), [6] proposed a stator multi-tooth structure applied to reduce a half of permanent magnets, as shown in Fig. 1(b). For the reduction of overall weight of the driving motor and easy installation, [7] proposed a modular rotor RFFSPMM in Fig. 1(c), which removed the traditional rotor yoke. The modular rotor FSPMM effectively provided the same torque as that provided by the traditional RFFSPMM while reducing iron loss.

In a stator-typed RFFSPMM, the permanent magnet is on the stator, and therefore the magnetic saturation of the stator is easily achieved and the space for armature winding slot is reduced. In Fig. 1(d), an inner rotor-typed FSPMM was proposed in [8], which compared the two structures of the permanent magnets on the rotor and stator. The results showed that the rotor-typed RFFSPMM could provide greater torque density. The outer rotor-type RFFSPMM was proposed in [9]. As shown in Fig. 1(e), the outer rotor-typed RFFSPMM was more efficiently cooled than the inner rotor-typed RFFSPMM. Moreover, the outer rotor-typed RFFSPMM reduced torque ripple, and improved efficiency and overload capability [9]. In order to widen the operation range and solve the problem of single permanent magnet excitation, RFFSPMM with hybrid excitation structures were researched in [10-11]. In Fig 1(f) and Fig. 1(g), the DC excitation and external mechanical flux adjuster were used to regulate magnetic field of RFFSPMM, respectively. It was found that the flux adjuster could provide more outstanding flux-weakening performance for wide-speed range operation.

AFFSPMMs have good application prospects in various fields, such as electric vehicle, ship propeller and wind power generation, due to its short axial dimension, large power/torque

Manuscript was submitted for review on 30, January, 2020.

This work was supported by the National Natural Science Foundation of China (51507087), the Six Talents Summit Project of Jiangsu Province (XNYQC-017) and the Science and Technology Planning Project of Nantong City (MS22019017 and JC2018145).

Xu Zhang is with Nantong University(e-mail: zhangxu_ele@126.com)

Wei Zhang is a professor in Nantong University(e-mail: zhang.w@ntu.edu.cn)

Xingyan Liang and Ping Lu are associate professors in Nantong University(e-mail: liang.xy@ntu.edu.cn, 642214336@qq.com)

Digital Object Identifier 10.30941/CESTEMS.2020.00024

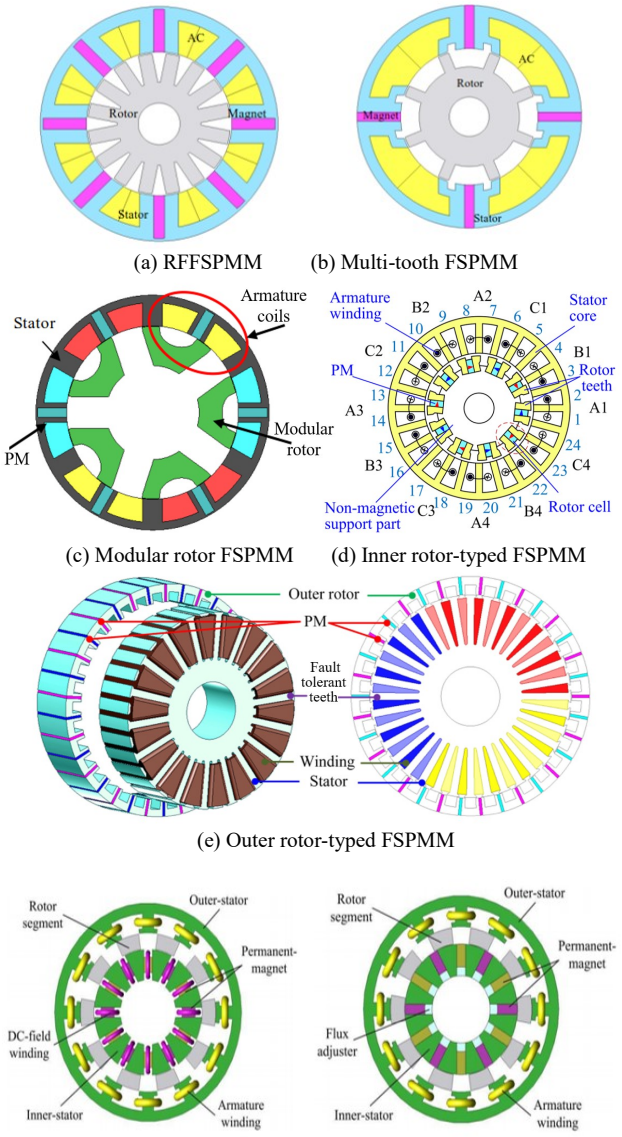


(a) RFFSPMM (b) Multi-tooth FSPMM

(c) Modular rotor FSPMM (d) Inner rotor-typed FSPMM

(e) Outer rotor-typed FSPMM

(f) DC field excitation FSPMM (g) Flux adjuster excitation FSPMM

Fig. 1. Different topologies of RFFSPMM.

density and high efficiency. In Fig. 2(a), U-, C- and E-typed AFFSPMMs were researched and compared in [12]. It was found that the C-core AFFSPMM had a higher torque output than E- and U-typed AFFSPMMs. Meanwhile, the E-typed AFFSPMM had better fault tolerance. To facilitate the direct drive of electric vehicles, the double-rotor structures of AFFSPMM were studied in [13]-[14]. It was found in [13] that the 12/13-pole AFFSPMM in Fig. 2(b) not only improved torque/power density but also reduced cogging torque and torque ripple. To increase space for windings and output torque capability, a novel yokeless and segmented armature axial field flux-switching sandwiched permanent magnet (YASA-AFFSSPM) was proposed in [14], as shown in Fig. 2(c). The space for winding was increased because of the absence of yoke in the stator. In addition, the even-order harmonics of the back-EMF were removed by the double unaligned rotors. It was shown in [14] that the YASA-AFFSSPM motor exhibited higher torque density and lower cogging torque than the AFFSSPM machine with yoke. However, the single magnetic excitation resulted in a small speed regulation range. To improve magnetic field adjustment capability, [15]-[17] proposed an E-core hybrid excitation AFFSPMM in Fig. 2(d). By applying excitation currents, the AFFSPMM increased the range of speed regulation and improved the output torque capability. However, the regulating range was limited by the excitation current. Axial magnetic flux-switching memory machine in Fig. 2(e) was proposed in [18]. Based on the high coercivity permanent magnets, the low coercivity permanent magnets in series were used to adjust the magnetic field easily through the application of pulse currents.

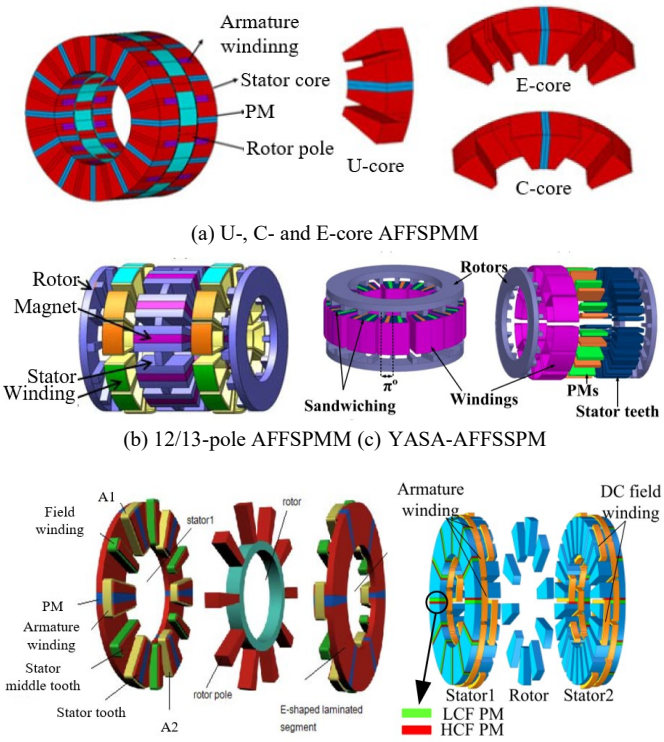


(a) U-, C- and E-core AFFSPMM

(b) 12/13-pole AFFSPMM (c) YASA-AFFSSPM

(d) hybrid excitation AFFSPMM (e) memory machine

Fig. 2. Different topologies of AFFSPMM.

According to above mentioned，the different stator- and rotor- typed FSPMMs have been proposed and researched, but merely few literature is available to compare axial and radial FSPM machines. Therefore, under the condition of the same outer diameters and volumes, the characteristics of the two types of H-core FSPM machines are mainly analysed and compared in this paper. The structures and principles of FSPM machines are introduced in Section II, and the design parameters are established. The performances in terms of air gap magnetic density, cogging torque, flux-linkage, back electromotive force, inductance, electromagnetic torque and loss in the two machines are analysed and compared in Section III. The related experiments are done for the AFFSPMM in Section IV. Finally, the conclusions are given in Section V.

## II. Topology And Operating Principle

### *A. Topology*

The three-dimensional structures of AFFSPMM and RFFSPMM are shown in Fig. 3 and 4，respectively. As shown

in Fig. 3, the AFFSPMM consists of double rotors and a single stator. The double rotors are placed symmetrically about the stator and mounted coaxially. The stator is composed of H-shaped stator cores, permanent magnets, armature windings, excitation windings and non-magnetic isolation blocks. The design of the non-magnetic isolation block increases the magnetic permeability of the phase-to-phase magnetic circuit and reduces the mutual inductance between adjacent coils. The armature winding is wound around the permanent magnet and the adjacent stator teeth of the two H-shaped cores. The excitation winding is wound around the permanent magnet and the two H-shaped cores. The excitation winding is located in the space between the two non-magnetic isolation blocks. The RFFSPMM is composed of a rotor and stator, and the stator is composed of H-shaped cores, permanent magnets, armature windings and excitation windings. The armature winding is wound around the permanent magnet and the adjacent stator teeth of two H-shaped cores. In addition, the excitation winding is wound around the H-shaped stator core, as shown in Fig. 4. For the two FSPM machines, the rotors are both simple and robust.

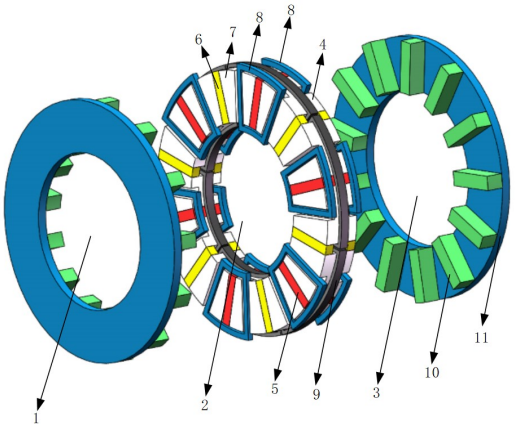


Fig. 3. Three-dimensional structure of AFFSPMM 1) rotor 1, 2) stator, 3) rotor 2, 4) H core, 5) permanent magnet, 6) non-magnetic isolating block, 7) stator tooth, 8) armature winding, 9) excitation winding, 10) rotor tooth and 11) rotor yoke.

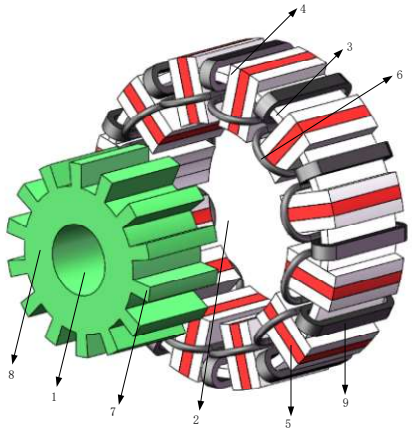


Fig. 4. Three-dimensional structure of RFFSPMM 1) rotor, 2) stator, 3) H-type core, 4) stator tooth, 5) permanent magnet, 6) armature winding, 7) rotor tooth, 8) rotor yoke and 9) excitation winding.

### *B. Operating Principle*

The principle of flux switching is depicted in Fig. 5(a)-(d). When the rotor of the machine rotates, the flux in the stator winding changes periodically. With the variation of the rotor from position1 to position4, the magnetic flux changes from the positive maximum value to the negative maximum value, completing flux-switching of a period.

The principle of hybrid excitation is depicted in Fig. 5(e)-(f). In Fig. 5(e)-(f), the solid line represents the direction of the magnetic field produced by the permanent magnets, and the dotted line shows the direction of the magnetic field excited by the DC field current. When the direction of the magnetic field generated by the DC excitation current coincides with the direction of the magnetic field generated by the permanent magnet, the strengthening flux is achieved in Fig. 5(e). Similarly, the weakening flux is realized through the reverse excitation current flowing into the field winding, as shown in Fig. 5(f).

In order to obtain large torque and reduced torque ripple, 6/13 AFFSPMM and 12/14 RFSPMM with the same total volumes under the condition of the same outer dimentions are optimized based on 3D finite element method [19], and the design parameters of the AFFSPMM and RFFSPMM are shown in TABLE I. Meanwhile, the main variables are marked in Fig. 5 and 6.

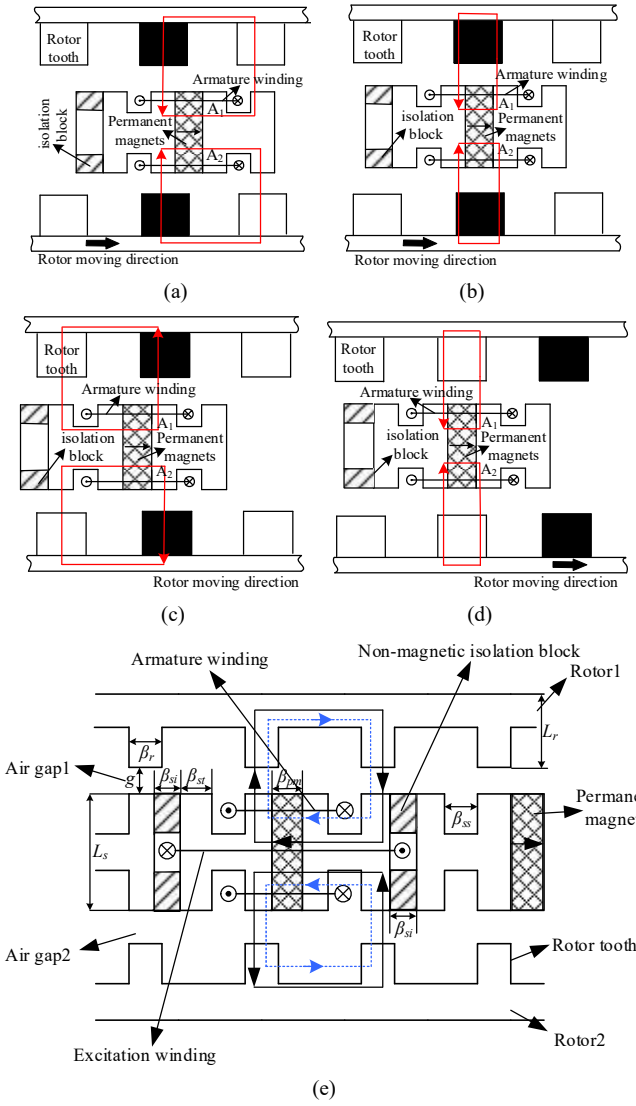

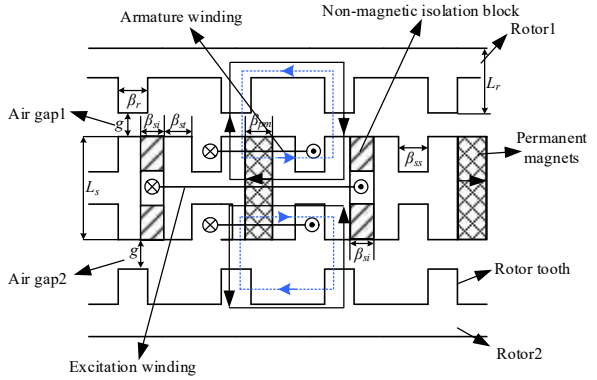


(f)

Fig. 5. Two-dimensional expansion diagram of AFFSPMM. (a) position1 at positive maximum flux (b) position2 at zero flux (b) position3 at negative maximum flux (d) position4 at zero flux (e) strengthening flux (f) weakening flux.

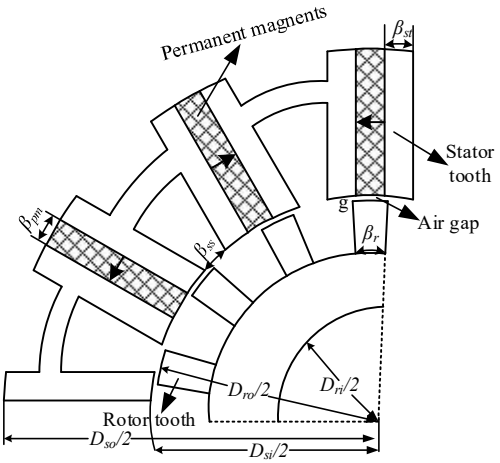


Fig. 6. 1/4 two-dimensional expansion diagram of RFFSPMM

TABLE I
DESIGN PARAMETERS OF TWO TYPE MACHINES

| Parameter | AFFSPMM | RFFSPMM |
|---|---|---|
| Stator/rotor pole | 6/13 | 12/14 |
| Rotor outer diameter $D_{ro}$ (mm) | 140 | 82.6 |
| Rotor inner diameter $D_{ri}$ (mm) | 84 | 10 |
| Rotor axial length $L_r$ (mm) | 12 | 40 |
| Phase winding turns | 42 | 21 |
| Slot filling factor（%） | 76 | 39 |
| Air gap length $g$ (mm) | 1 | 0.2 |
| Stator isolating block width $\beta_{si}$ (°) | 7.5 | - |
| Stator outer diameter $D_{so}$ (mm) | 140 | |
| Stator inner diameter $D_{si}$ (mm) | 84 | |
| Stator axial length $L_s$ (mm) | 40 | |
| Permanent magnet width $\beta_{pm}$ (°) | 7.5 | |
| Stator tooth width $\beta_{st}$ (°) | 7.5 | |
| Rotor tooth width $\beta_r$ (°) | 10.5 | |
| Rated speed n (r/min) | 750 | |
| Rated power (W) | 350 | |
| Total volume ($m^3$) | 0.000506 | |

## III. PERFORMANCE ANALYSIS AND COMPARISON

### A. Air Gap Magnetic Density

Fig. 7(a) shows the air gap magnetic density waveforms of the two machines. Fig. 7(a) shows that the two types of machines have focused magnetic characteristics and their peak values of air-gap magnetic density are both around 1.5T. Based on the Fourier analysis, the harmonic analysis of the magnetic densities are shown in Fig. 7(b). The fundamental flux density of AFFSPMM is found to be 0.4845T and that of RFFSPMM is 0.7685T. However, the permanent magnet usage amount of RFFSPMM is about twice of the AFFSPMM. Therefore, the AFFSPMM has a higher permanent magnet utilization rate.

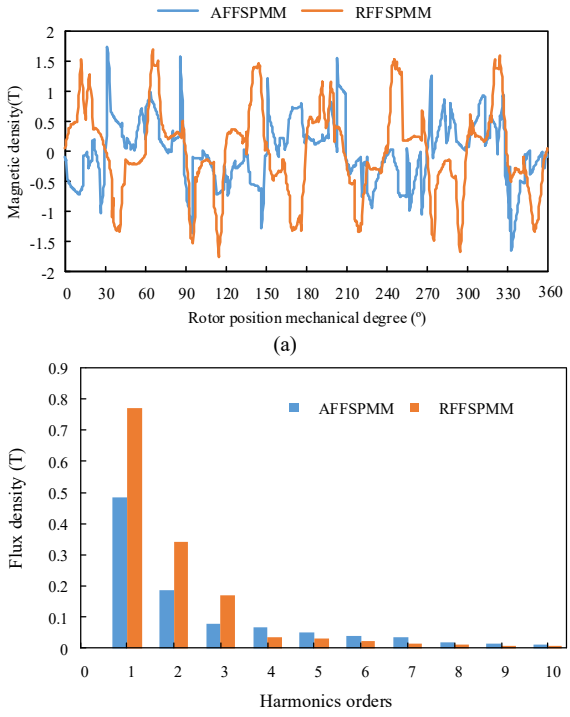


Fig. 7. Air gap magnetic density (a) waveform of air gap magnetic density (b) harmonic analysis.

### B. Cogging Torque

The cogging torque waveforms of the two machines are presented in Fig. 8. The peak–peak values of cogging torque of the AFFSPMM and RFFSPMM are 1.4 N·m and 1.8 N·m, respectively in Fig. 8. Due to the more permanent magnet usages, the RFFSPMM has larger cogging torque than AFFSPMM.

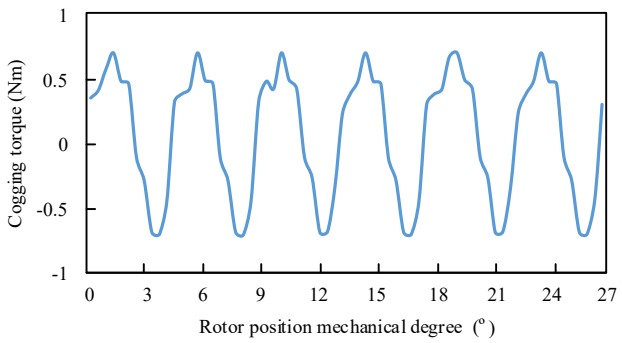

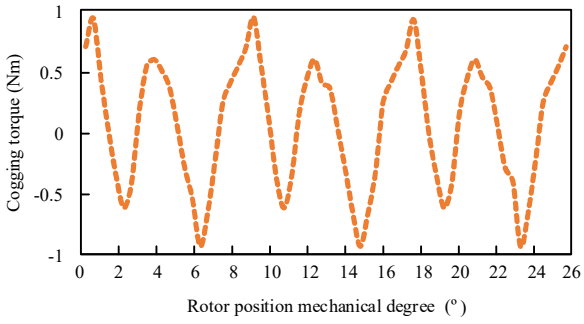


(b)

Fig. 8. Cogging torque. (a)AFFSPMM (b) RFFSPMM

### C. Flux-linkage and Back Electromotive Force

To obtain similar flux linkages and back EMF at the same rated speed, the armature winding turns of the AFFSPMM and RFFSPMM are designed. Fig. 9(a) and 9(b) show the flux linkage and no-load back EMF waveforms of the two machines at the rated speed of 750 r/min, respectively. Fig. 9 shows that the two machines can obtain approximately equal flux linkages and back EMF values. Fig. 9(c) shows the harmonic analysis of the back EMF of the two type machines. It is found that the values of THD in RFFSPMM and AFFSPMM are 6.78% and 4.47%, respectively, which indicates that the AFFSPMM can achieve more sinusoidal back EMF waveform.

### D. Self-inductance and Mutual Inductance

The inductance is a key parameter that has a direct impact on the motor performance. Table II shows the values of the self-inductance and mutual inductance of the two machines.

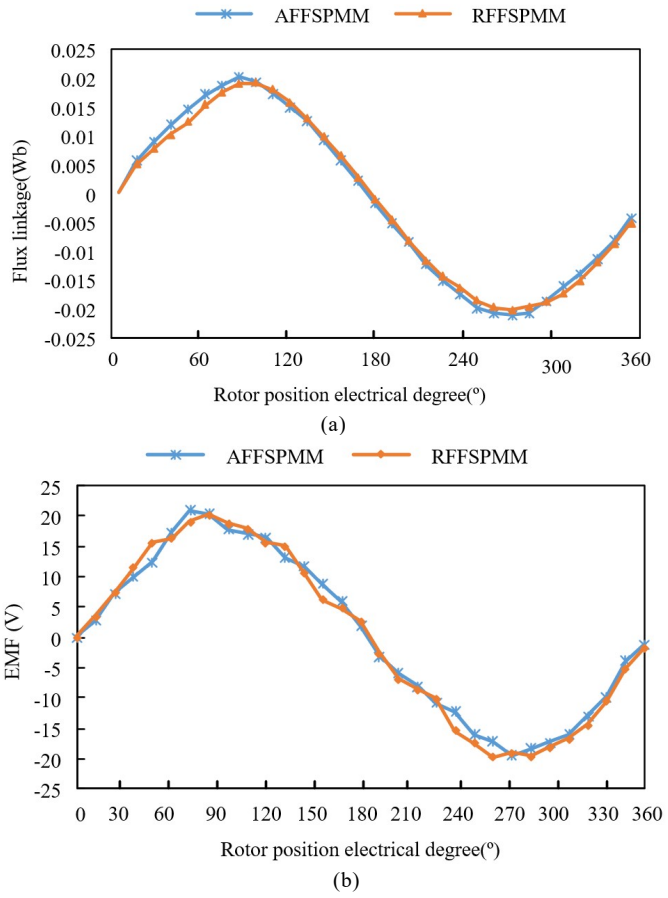


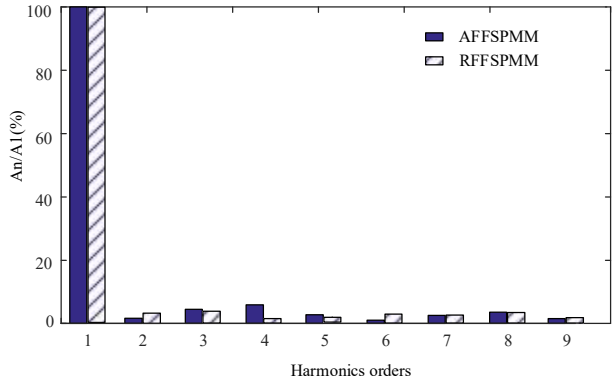


(c)

Fig. 9. Flux-linkage and back EMF waveforms (a) Flux-linkage (b) Back EMF (c) Harmonic analysis of back-EMF

Table II shows that the self-inductance of AFFSPMM is 2.87mH, the mutual inductance of AFFSPMM is 0.136 mH and the ratio of the mutual inductance to self-inductance is 4.7%. The self-inductance and mutual inductance of RFFSPMM is 0.896 and 0.379mH, respectively. Moreover, the ratio of the mutual inductance to self-inductance is 42.37%. The large self-inductance is beneficial to suppress the short-circuit current, and the low mutual inductance and self-inductance ratio is beneficial to suppress the influence of the fault phase on the normal phase. Therefore, the AFFSPMM has better fault tolerance than the RFFSPMM.

TABLE II
INDUCTANCE PARAMETERS OF THE TWO MACHINES

| Motor type | Self-inductance (mH) | Mutual inductance (mH) | Mutual-/self-inductance (%) |
|---|---|---|---|
| AFFSPMM | 2.87 | 0.136 | 4.7% |
| RFFSPMM | 0.896 | 0.379 | 42.38% |

### E. Electromagnetic Torque

Without considering DC excitation, the electromagnetic torque at different speeds is shown in Fig. 10, the rated torques of AFFSPMM and RFFSPMM are both approximately 4.5 N·m, and the two machines have similar constant torque region. During the constant power region, the AFFSPMM can provide a greater torque output than RFFSPMM.

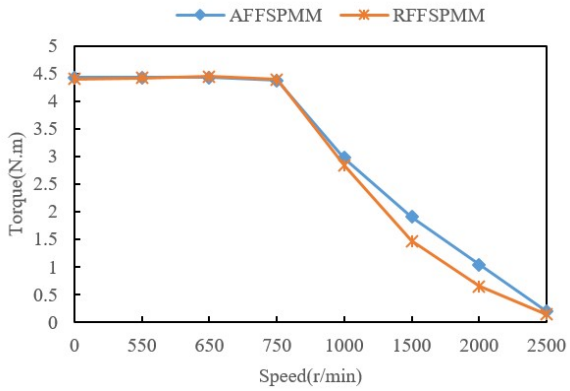


Fig. 10. Torque characteristic.

### F. Copper Loss

According to (1), the copper loss of the two machines are calculated and listed in Table III.

$$P_{Cu} = mI^2R \tag{1}$$

where $m$ is the number of motor phases, $I$ is the current effective value and $R$ is the resistance value of each phase winding.

TABLE III
COMPARISON OF COPPER LOSS UNDER THE RATED LOAD

| Copper loss | AFFSPMM | RFFSPMM |
|---|---|---|
| Theoretical results (W) | 14.32 | 9.036 |
| Simulation results (W) | 14.79 | 10.12 |

Table III shows copper loss of the machines when the load is 4.5 N·m. Theoretical values of copper loss of AFFSPMM and RFFSPMM are calculated, and compared with their simulation results in TABLE III. It is found in TABLE III that the simulation results are similar to the theoretical calculation results，and the copper loss of AFFSPMM is higher than that of RFFSPMM.

### *G.Iron Loss*

The stator and rotor cores stacked with silicon steel sheets are repeatedly magnetised in an alternating electromagnetic field, so the magnetic domains in the silicon steel sheets rub against each other, which results in irreversible stator and rotor iron loss [20].

The iron loss can be got by (2).

$$P_{Fe} = P_h + P_e + P_{exc} \tag{2}$$

The hysteresis loss $P_h$ is obtained by (3).

$$P_h = f\int HdB = K_h f B_m^a \tag{3}$$

where $K_h$ is hysteresis loss coefficient, $a$ is hysteresis loss calculation parameter, $f$ is magnetic field change rate and $B_m$ is magnetic density amplitude. $K_h$ and $a$ are parameters related to the material properties of the silicon steel sheet, which can be obtained from the P–H curve.

Eddy current loss $P_e$ can be calculated by (4).

$$P_e = \frac{\sigma\delta^2}{12\rho T}\int_0^T\left(\frac{dB(t)}{dt}\right)dt \tag{4}$$

where $\sigma$ is the conductivity of the silicon steel sheet, $\delta$ is the thickness of silicon steel sheet and $\rho$ is the density of the silicon steel sheet.

Assuming the magnetic field in the eddy current region satisfies (5) and (6), (7) is obtained by the Kircoff equation [21].

$$\nabla\bullet\left(\frac{1}{\mu}\nabla\times A\right) = J_a - \sigma\left(\frac{\partial A}{\partial t} + \nabla\phi\right) + \frac{1}{\mu_0}\nabla\times M \tag{5}$$

$$\nabla\bullet\left[\sigma\left(\frac{\partial A}{\partial t} + \nabla\phi\right)\right] = 0 \tag{6}$$

$$V_a = \frac{d\psi}{dt} + R_a i_a \tag{7}$$

where $A$ is vector position, $\phi$ is scalar potential, $J_a$ is armature current density, $\mu$ is permeability, $\sigma$ is conductivity, $M$ is magnetization of permanent magnet, $\Psi$ is armature winding flux linkage, $V_a$ and $i_a$ are armature voltage and current, respectively.

The eddy current loss of the permanent magnet can be obtained as (8).

$$W_{mag} = \frac{1}{T}\int_0^T\int_{Vm}\sigma\left|\frac{\partial A}{\partial t} + \nabla\phi\right|^2 dvdt \tag{8}$$

where $T$ is the calculation time, $V_m$ is the volume of permanent magnet.

The additional loss $P_{exc}$ is given in (9).

$$P_{exc} = \frac{\sqrt{\sigma G V_0 S}}{\rho T}\int_0^T\left|\frac{dB(t)}{dt}\right|^{1.5} dt \tag{9}$$

where $G$ and $V_0$ are silicon steel sheet related parameters， and $S$ is cross-sectional area.

TABLE IV
COMPARISON OF LOSS AT NO LOAD AND RATED LOAD

| | No load | | Rated load | |
|---|---|---|---|---|
| | AFFSPMM | RFFSPMM | AFFSPMM | RFFSPMM |
| Iron loss (W) | 4.34 | 7.81 | 11.41 | 17.01 |
| Copper loss (W) | 1.63 | 0.53 | 14.79 | 10.12 |
| Eddy current loss (W) | 1.65 | 3.84 | 5.04 | 7.54 |
| Total loss (W) | 7.62 | 12.18 | 31.24 | 34.67 |

Under the condition of no load and rated load, the different losses are obtained from TABLE IV. TABLE IV shows that the total losses of the AFFSPMM and RFFSPMM are 7.65W and 12.18W at no load, respectively. When the machines run at the rated load and speed, the total losses of AFFSPMM and RFFSPMM are 31.24W and 34.67W, respectively. Therefore, the total losses of RFFSPMM are both higher than those of AFFSPMM at no load and rated load.

## IV. EXPERIMENT RESULTS

In order to validate the finite element results, the experimental platform is built for the AFFSPMM, as shown in Fig. 11. The experimental platform mainly includes a controller dSPACE1104, control circuit with six IGBT switch tubes, control conditioning board, current sensor, magnetic power brake, and AFFSPMM. At the rated speed, no-load back-EMF is tested and shown in Fig. 12(a), which is similar close to the finite element result of AFFSPMM in Fig. 9(b). The phase current, rotor speed and electromagnetic torque at rated load are tested and shown in the Fig. 12(b), which indicate the AFFSPMM can operate stably at the rated load.

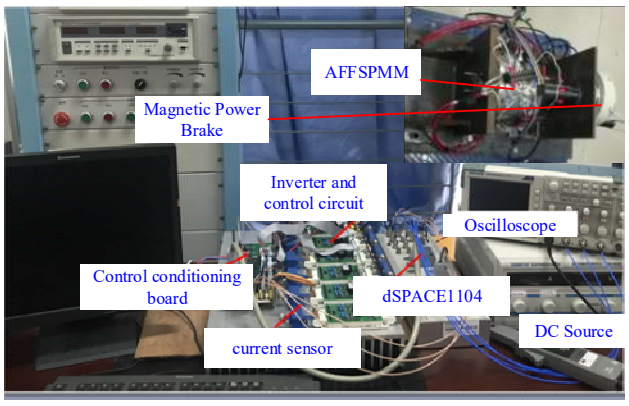


Fig. 11. Experimental platform.

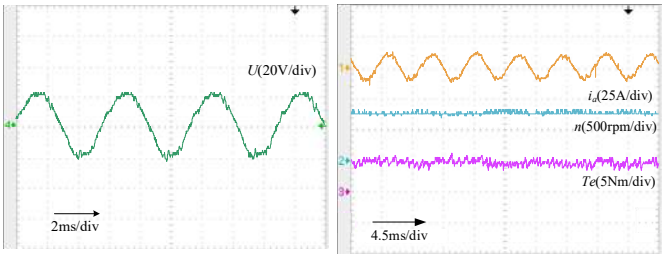


(a) no-load back EMF (b) torque at rated load

Fig. 12. Experiment waveforms.

## V. CONCLUSION

In the paper, the performances of two new types of FSPM machines with the same total volumes are compared and analyzed through the finite element method under the condition of the same outer diameters. The results show that the AFFSPM and RFFSFM machines have strong focusing magnetic characteristic, and the fundamental flux density of RFFSPMM is 37% larger than that of AFFSPMM. However, the RFFSPMM has a half more permanent magnet volumes than AFFSPMM. Meanwhile, the two machines have similar constant torque range, but the AFFSPMM can provide larger torque density than RFFSPMM in the constant power area. In addition, the ratio of the mutual- to self-inductance of AFFSPMM is 37.68% smaller than that of RFFSPMM, which is beneficial to improve the fault tolerance. The AFFSPMM can obtain higher efficiency than RFFSPMM although the copper loss of AFFSPMM is larger than that of RFFSPMM at the rated load. Considering the price of silicon steel sheet is much lower than that of permanent magnet, it is found that the AFFSPMM can get better performances than the RFFSPMM while reducing the cost.

## REFERENCES

[1] Charadsuksawat, Y. Laoonual and N. Chollacoop, "Comparative Study of Hybrid Electric Vehicle and Conventional Vehicle Under New European Driving Cycle and Bangkok Driving Cycle," in *Proc. 2018 IEEE Transportation Electrification Conference and Expo, Asia-Pacific (ITEC Asia-Pacific)*, Bangkok, 2018, pp. 1-6.

[2] A. M. Lulhe and T. N. Date, "A technology review paper for drives used in electrical vehicle (EV) & hybrid electrical vehicles (HEV)," in *Proc. 2015 International Conference on Control, Instrumentation, Communication and Computational Technologies (ICCICCT)*, Kumaracoil, 2015, pp. 632-636..

[3] H. Zheng, C. Wei, D. Sun, Y. Ren, L. Zeng and R. Pei, "Rotor Design of Permanent Magnet Synchronous Reluctance Motors in Rail Traffic Vehicle," in *Proc. 2018 21st International Conference on Electrical Machines and Systems (ICEMS)*, Jeju, 2018, pp. 2762-2765.

[4] A. M. Omara and M. A. Sleptsov, "Performance assessment of battery-powered electric vehicle employing PMSM powertrain system," in *Proc. 2017 IEEE Conference of Russian Young Researchers in Electrical and Electronic Engineering (EIConRus)*, St. Petersburg, 2017, pp. 963-968.

[5] H. Q. Nguyen, J. Jiang and S. Yang, "Design of a 12-slot 7-pole wound-field flux switching motor for traction applications," in *Proc. 2016 IEEE International Conference on Industrial Technology (ICIT)*, Taipei, 2016, pp. 1275-1280.

[6] L. I. Jusoh, E. Sulaiman, E. Mbadiwe and H. A. Soomro, "Design of Multi-tooth Permanent Magnet Flux Switching Machine for Electric Bicycle Application," in *Proc. 2019 IEEE 15th International Colloquium on Signal Processing & Its Applications (CSPA)*, Penang, Malaysia, 2019, pp. 174-177.

[7] I. A. Soomro, E. Sulaiman and H. A. Soomro, "Modular rotor Based Permanent Magnet Flux Switching Machine for Light Weight EV," in *Proc. 2019 IEEE 15th International Colloquium on Signal Processing & Its Applications (CSPA)*, Penang, Malaysia, 2019, pp. 182-185.

[8] P. Su, W. Hua, Z. Wu, Z. Chen, G. Zhang and M. Cheng, "Comprehensive Comparison of Rotor Permanent Magnet and Stator Permanent Magnet Flux-Switching Machines," *IEEE Transactions on Industrial Electronics*, vol. 66, no. 8, pp. 5862-5871, 2019.

[9] L. Mo, T. Zhang and Q. Lu, "Design and Analysis of an Outer-Rotor-Permanent-Magnet Flux-Switching Machine for Electric Vehicle Applications," *IEEE Transactions on Applied Superconductivity*, vol. 29, no. 2, pp. 1-5, 2019.

[10] Y. Maeda, T. Kosaka and N. Matsui, "Design study on hybrid excitation flux switching motor with permanent magnet placed at middle of field coil slot for HEV drives," in *Proc. 2016 XXII International Conference on Electrical Machines (ICEM)*, Lausanne, 2016, pp. 2522-2528.

[11] C. H. T. Lee, J. L. Kirtley and M. Angle, "A Partitioned-Stator Flux-Switching Permanent-Magnet Machine With Mechanical Flux Adjusters for Hybrid Electric Vehicles," *IEEE Transactions on Magnetics*, vol. 53, no. 11, pp. 1-7, 2017.

[12] W. Zhang, X. Liang and M. Lin, "Analysis and Comparison of Axial Field Flux-Switching Permanent Magnet Machines With Three Different Stator Cores," *IEEE Transactions on Applied Superconductivity*, vol. 26, no. 7, pp. 1-6, 2016.

[13] W. Zhao, T. A. Lipo and B. Kwon, "A Novel Dual-Rotor, Axial Field, Fault-Tolerant Flux-Switching Permanent Magnet Machine With High-Torque Performance," *IEEE Transactions on Magnetics*, vol. 51, no. 11, pp. 1-4, 2015.

[14] J. R. Fard and M. Ardebili, "Design and Control of a Novel Yokeless Axial Flux-Switching Permanent-Magnet Motor," *IEEE Transactions on Energy Conversion*, vol. 34, no. 2, pp. 631-642, 2019.

[15] D Xu, M Lin , X Fu, L Hao , J Zhao. "Characteristics and experimental study of a hybrid excitation axial magnetic field flux switching permanent magnet motor", *Motor and Control Applications*, , vol. 44, no. 11, pp. 100- 105, 2017.

[16] W. Zhang, X. Liang and F. Yu, "Fault-Tolerant Control of Hybrid Excitation Axial Field Flux-Switching Permanent Magnet Machines," *IEEE Transactions on Magnetics*, vol. 54, no. 11, pp. 1-5, 2018.

[17] W. Zhang, X. Liang, M. Lin, L. Hao and N. Li, "Design and Analysis of Novel Hybrid-Excited Axial Field Flux-Switching Permanent Magnet Machines," *IEEE Transactions on Applied Superconductivity*, , vol. 26, no. 4, pp. 1-5, 2016.

[18] N Li, X Fu, J Zhu, M Lin, G Yang, Y Kong, L Hao. "Hybrid-Excited Series Permanent Magnet Axial Field Flux Switching Memory Machine", *IEEE Transactions on Applied Superconductivity*, vol. 29, no. 2, 2019.

[19] X. Zhang, W. Zhang and F. Yu, "Optimal Design of a Hybrid Excitation Axial Flux-Switching In-Wheel Motor," in *Proc. 2018 Asia-Pacific Magnetic Recording Conference (APMRC)*, Shanghai, 2018, pp. 1-2.

[20] W. Tong, Y. Wang, R. Sun, S. Wu and J. Jia, "Simulation and Experimental Study on No-Load Loss Distributions of an IPM Motor Under the Conditions of Both Sinusoidal Supply and Converter Supply," *IEEE Transactions on Magnetics*, vol. 54, no. 11, pp. 1-6, 2018

[21] G. Jang, M. Koo, J. Kim and J. Choi, "Analysis of Eddy Current Loss in Permanent Magnet Linear Synchronous Generator Considering Tapped Holes in Movers Using Semi-3-D Analytical Method," *IEEE Transactions on Magnetics*, vol. 53, no. 11, pp. 1-5, 2017.

**Xu Zhang** was born in Suqian, Jiangsu, China in 1993. He received the B. Sc. degree in electrical engineering from Jincheng College of Nanjing University of Aeronautics and Astronautics, China, in 2017, and currrntly working toward the M. Sc. degree in Control Science and Engineering in Nantong University, Nantong, China. His current major research interest is electromagnetic design and multi-objective optimization of axial field flux-switching permanent magnet machine.

**Wei Zhang** was born in Taizhou, Jiangsu, China in 1977. She received the B. Sc. degree in electrical engineering from Nantong University, Nantong, China, in 2000, and the M. Sc. degree and the Ph. D. degree in electrical engineering from Southeast University, Nanjing, China, in 2007 and in 2016, respectively. Since 2000, she has been with Nantong University where she is a professor in the college of electrical engineering. From January 2017 to December 2017, she was a visiting scholar at the University of Sheffield, Sheffield, UK. Her current major research interests include design and control of permanent magnet brushless machines and drives for automotive applications, and renewable energy applications.

**Xingyan Liang** was born in Nantong, Jiangsu, China in 1977. He received the B. Sc. degree and the M. Sc. Degree in electrical engineering from Jiangsu University, Zhenjiang, China, in 1998 and in 2004. Science 1998, he has been with Nantong University where he is a associate professor in the School of Information Science and Technology. His current major research interest is the design of intelligent motor controller and IoT application.

**Ping Lu** was born in Nantong, Jiangsu, China in 1972. He received the B. Sc. degree in electrical engineering from Nantong University, Nantong, China, in 1996, and the M. Sc. Degree in school of automation from Nanjing University of Science & Technology, Nanjing, China, in 2004. Science 1996, he has been with Nantong University where he is a associate professor in the college of electrical engineering. His current major research interest is intelligent control and parameter identification.